*Cell Tissue Kinet.* (1986), **19**, 627-645

54

# Intestinal cell proliferation. I. A comprehensive model of steady-state proliferation in the crypt

M. Loeffler*, R. Stein*, H.-E. Wichmann†, C. S. Potten‡, P. Kaur‡ and S. Chwalinski‡

**Universitaetsklinik Koeln Medizinische Klinik I, LFI-EDV, Joseph-Stelzmann-Str. 9, D-5000 Koeln 41, West Germany, †Institut fuer Umwelthygiene, Auf'm Hennekamp 50, D-4000 Duesseldorf 1, West Germany and ‡Paterson Laboratories, Christie Hospital, Manchester M20 9BX, U.K.*

(*Received 20 May 1985; revision accepted 18 July 1985*)

**Abstract.** Cell replacement in the crypt of the murine small intestine has been studied and modelled mathematically under steady-state conditions. A great deal of information is available for this system, e.g. cell cycle times, S phase durations, the rate of daily cell production, the Paneth cell distribution etc. The purpose of the present work was to consider simultaneously as much of these data as possible and to formulate a model based upon the behaviour of individual cells which adequately accounted for them. A simple mathematical representation of the crypt has been developed. This consists of sixteen stem cells per crypt ($T_C = 16$ hr, $T_S = 9$ hr), and four subsequent transit cell divisions ($T_C = 11$ to 12 hr, $T_S = 8$ hr) before maturation. Experimental data considered to test the modelling were LI and data on the number of vertical runs of similarly labelled cells. All data were obtained from the ileum after 25 $\mu$Ci [$^3$H]TdR given at 09.00 hours. A number of alternative assumptions have been considered and either accepted or rejected. Two alternative model concepts of cell displacement explain the data equally well. One is dependent upon strong local cell generation age determinance while the other could accommodate any weak local cell displacement process in conjunction with an environmental cut-off determinant at the middle of the crypt. Both models provide new interpretations of the data, e.g. certain rates of lateral cell exchange between neighbouring columns (250 to 350 per crypt per day out of a total of 420 cell divisions per day) can be concluded from run data, while LI data provide information about the mechanisms involved in maintaining a position-related age order in the crypt.

Although extensive research has been undertaken to study the cell kinetics in the crypts of the small intestine, the following questions have so far resisted a clear answer: How many stem cells does each crypt contain? How many cell divisions occur in the transit population and is this number rigidly fixed? What is the average cell cycle time of the stem cells and its phase durations? How precisely do the cell kinetics vary with the position of a cell within the crypt and within a cell hierarchy? Is there a kinetic heterogeneity in the stem or transit populations? What

Correspondence: M. Loeffler, Medizinische Klinik 1, LFI-EDV, Joseph-Stelzmann-Strasse 9, D-5000 Koeln 41, West Germany.

mechanisms are involved in cell migration and how is this related to proliferation? How extensive is lateral compared with vertical cell displacement? Do local or global mechanisms determine the boundary between proliferating and maturing cells? The purpose of the present work was to construct a mathematical model for the steady state so that some of the questions outlined above could be investigated by comparing model predictions with actual experimental data from the ileum and by testing alternative concepts. The model should account for the characteristics of individual cells and should relate to the crypt geometry. Furthermore, it should provide an understanding of how labelling experiments (LI, number of vertical runs of like-labelled cells) are affected by the constant movement of cells in the crypt.

## THE MODEL

A model of cell proliferation in intestinal crypts has to take several things into account. For each of these we first summarize the biological knowledge under a heading (i); we then describe (under the heading (ii)) the basic assumptions for the reference model. The mathematical procedure is outlined under heading (iii) and may be omitted by the non-mathematical reader. Under heading (iv) we indicate alternative assumptions.

### 1. Architecture of the mouse crypt

(i) The average mouse crypt contains about sixteen columns of cells in circumference. The crypt/villus junction is somewhat ill-defined and open to subjective interpretation but may be between 20 and 25 cell positions from the base. The cell population in the crypt is not homogeneous. The lowermost region (up to position 7) contains Paneth cells and the crypt stem cells. The middle region (position 7 to 16) contains the rapidly cycling transit cells while the upper region (above position 16) consists largely of migrating postmitotic cells. These leave the crypt and migrate onto the villi where they are joined by the migrating cells of six to ten adjacent crypts. Most of these data come from many sources and are summarized in Potten & Hendry, 1983; Potten *et al.*, 1983; Wright & Alison, 1984. The number of stem cells per crypt and the number of transit cell divisions is not precisely known.

(ii) The model crypt will be considered as a cylinder of cells. Figure 1 shows the cylinder opened and rolled out flat as a $16 \times 24$ matrix of equally sized cells. The matrix can be expanded up to $16 \times 50$ to consider the vertical movements of cells out of the crypts. Any variations in the crypt diameter from the bottom to the top were not taken into account except for the very lowest cell position where the crypt tapers. Cell positions 1 to 6 may contain Paneth cells (P-cells). They were distributed according to a measured Paneth cell distribution (Table 1). In each column, stem cells (A-cells) may occupy the position immediately above the Paneth cells. Both cell types were regarded as non-migratory. Thus, a crypt could contain a maximum of sixteen stem cells. The next cell positions were occupied by several generations of proliferating transit cells (T-cells: T1, T2, T3, etc.) above which post-mitotic cells (M-cells) can be found (Fig. 1). All other cell types, e.g. goblet or enteroendocrine cells were neglected.

(iii) The cell positions in the crypt were represented by a two-dimensional time-dependent matrix $A(i, j/t)$ ($i$ refers to the column number 1–16, $j$ to the row number 1–50). The values of $A(i, j/t)$ code information about the generation type (P, A, T1, T2, T3, T4, M) at position $(i, j)$ at time $t$. Since the crypt has a cylindrical shape the first and last columns were treated as adjacent (cyclical boundary conditions). For each column the number of P-cells at the bottom was selected by a random number generator which had to fulfill the following conditions: (a) the number of P-cells in column $j+1$ must not differ from that in column $j$ by more than $+/-1$. The process starts with four or five P-cells in column 1; (b) the number of P cells must remain within

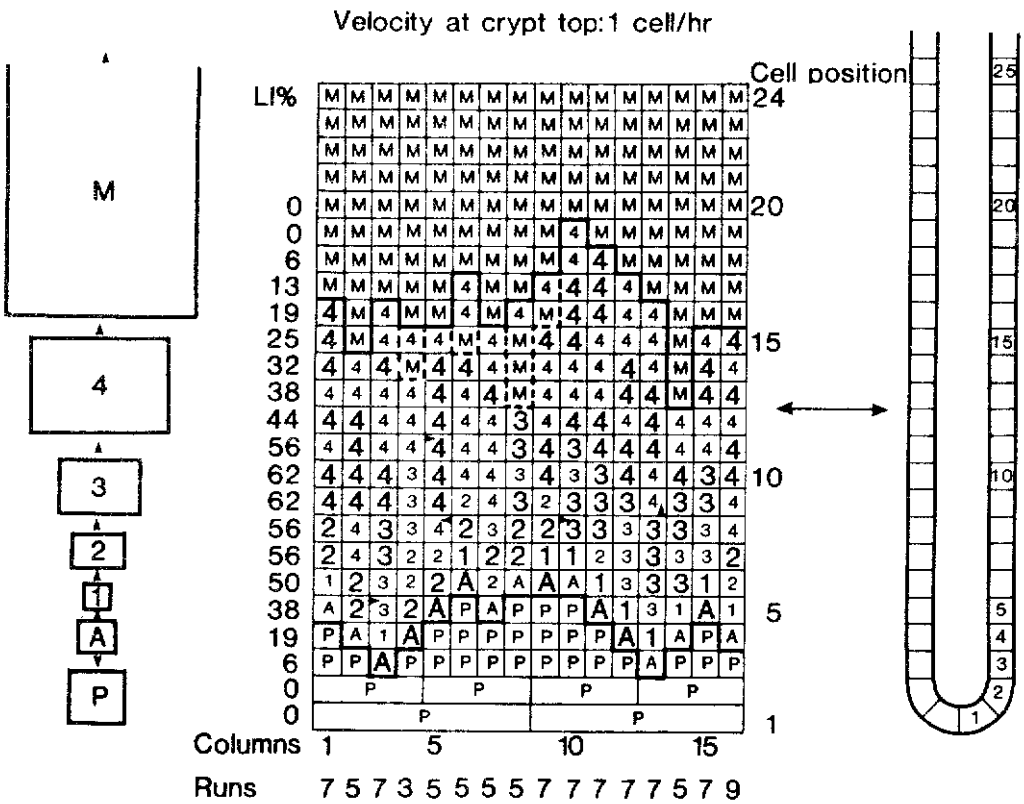


**Fig. 1.** Representation of the model crypt (reference model E). A crypt of sixteen cells in circumference is represented as opened and rolled out. Cells are located on a rectangular matrix: P, Paneth cells; A, stem cells; 1–4, transit cells (T-cells); M, mature cells. The large numbers indicate cells that have just become labelled by thymidine incorporation. The resulting LI values per row and the number of runs per column can be seen. The labelling index (LI) quantifies the percentage of labelled cells in a row. A run is defined as an unbroken sequence of labelled or unlabelled cells in a column (e.g. 7 runs in the first column). The arrow heads indicate some of the cells which may divide in the next hour and the direction of the arrow head indicates where the daughter cell will be placed (beneath the oldest of three neighbours to the right, left, top; in model F displacements to the top right and top left are also possible). The three examples on the left illustrate how sequences of labelled or unlabelled cells can be broken up such that the number of runs would increase in these columns. The other two examples would not change the number of runs. The displacement mechanism tends to eliminate cell generation heterogeneity in a row. (Thus, e.g. in row 8 column 5–7 the sequence will change from 4, 2*, 3 to 3*, 3*, 3 where * indicates label, i.e. heavy print in the figure.) In column 13, row 8 one finds an example where the model displacement does not eliminate local heterogeneity. The type 3 cell divides and a new type 4 cell is shifted upwards but one cell remains producing 3, 4*, 3. It should be noted that the local age-dependent displacement process generates a rather age-ordered matrix. With few exceptions older cells are placed on top of younger cells. Therefore, the 'skyline' of the highest type 4 cells (——) and the lowest type M cells (– – –) almost coincide. The M/T junction is rather well defined. The arrow between positions 12 and 13 indicates the possible position of an environmental influence, referred to as a 'cut-off' mechanism. The left-hand side illustrates the cellular hierarchy and the generation ages. The right-hand side schematically represents a crypt section. The matrix is based on a model suggested in Potten *et al.* (1982).

**Table 1.** The percentage of Paneth cells at each cell position

| Crypt position | Model* | Experiment† |
|---|---|---|
| 1 | 95 | 75 |
| 2 | 88 | 71 |
| 3 | 73 | 68 |
| 4 | 48 | 60 |
| 5 | 28 | 45 |
| 6 | 11 | 21 |
| 7 | 0 | 5 |
| 8 | 0 | 0 |

* For the model, ten individual crypts (160 columns) were simulated and compared to 100 experimental crypt sections.

† Determined from H + E stained 1 μm resin sections (S. Chwalinski, unpublished data).

the limits 1 to 6. This process produced a range of P-cell distributions whose median was very similar to that measured (Table 1).

The stem cells (A-cells) were placed on top of the Paneth cell distribution. If less than sixteen stem cells were chosen the procedure was: (a) one A-cell was placed into each local minimum of the P-cell distribution; (b) the remaining A-cells were distributed at random. Once A-cells were assigned to their places they remained there, keeping their generation index while one of their daughter cells receives the index of the first differentiating cell generation (i.e. 1).

(iv) Alternative calculations are performed with different Paneth cell distributions.

**2. Cell cycle parameters**

(i) Postmitotic cells do not divide. The Paneth cell turnover time is probably longer than 10 days (Devik & Iversen, 1970; Cheng & Leblond, 1974). This is very long compared with the cell cycle time in the mid crypt of about 12 hr, known from PLM and other data (Devik & Hagen, 1973; Kovacs & Potten, 1973; Al-Dewachi *et al.*, 1979; Tsubouchi & Potten, 1985). There is little evidence of any differences in the cell cycle amongst transit cells. The S phase constitutes slightly more than half of the cell cycle. A computer-aided cell phase estimate from PLM data for the middle of the crypt (Tsubouci & Potten, 1985) revealed similar values after labelling with 2·5 μCi or 100 μCi of [$^3$H]TdR ($T_S = 7$ hr, $T_{G_2+M} = 1{\cdot}5$ hr, $T_{G_1} = 4$ hr, $T_C = 12{\cdot}5$ hr, with variances of between 0·3 and 0·5 hr). The cell cycle time of stem cells is not known precisely, because no labelling techniques measure pure stem cell populations. A detailed PLM analysis of the cells at cell position 1–4 using 25 μCi [$^3$H]TdR provided estimates of $T_S = 8{\cdot}5$ hr, $T_{G_2+M} = 3$ hr, $T_{G_1} = 4{\cdot}5$ hr, $T_C = 16$ hr (Tsubouchi, Potten & Chadwick, unpublished data).

(ii) In the model we assumed that P and M-cells do not divide. The stem cells were given an average cell cycle time of 16 hr. The first two transit cell generations were assumed to have $T_C = 12$ hr, while the subsequent two generations have $T_C = 11$ hr. The duration of the S phase was assumed to be 9 hr for stem cells and 8 hr for transit cells. The mitotic-phase was assumed to last 1 hr. The time for $T_{G_1}$ was fixed at 2 hr for A-cells and 1 for T-cells (Table 2).

(iii) The cell cycle age of the cell at a position $(i, j)$ is represented by the matrix $B(i, j/t)$. The numerical values indicate how remote the cell is from its next division (e.g. if $B(5, 9/t) = 6$ the cell in column 5 and position 9 has 6 hr to go until it divides). The model was iterated at an

**Table 2.** Cell cycle times (hr)

| | Model* | | Experimental† | |
|---|---|---|---|---|
| | Stem cells | Transit cells | Stem cells (position 1–4) | Transit cells (position 13–16) |
| $T_C$ | 16 | 11–12 | 16 | 12·5 |
| $T_S$ | 9 | 8 | 8·5 | 7 |
| $T_{G_2+M}$ | 3 | 2 | 3 | 1·5 |
| $T_{G_1}$ | 4 | 2 | 4·5 | 3·5 |

* These model parameters are constants. Only $T_{G_1}$ may vary by 100% and this variation is selected at the beginning of each cell cycle by a random process. Thus, $T_{CA}$ varies between 12 and 20 hr stochastically and $T_{CT}$ between 10 and 14 hr.

† Parameters are derived from PLM, LI and MI data in the literature (Tsubouchi & Potten, 1985; Al-Dewachi *et al.*, 1979; Potten *et al.*, 1974) or from unpublished data (Tsubouchi, Potten & Chadwick).

increment of 1 hr. Every hour the cell cycle age index was reduced by 1 hr as cells approached mitosis ($B(i, j/t+1) = B(i, j/t) - 1$ if $B(i, j/t) > 1$). Consequently all times used in the model had to be integers. If two cells were born in the last step they were given a new generation index $A(i, j/t)$ (see above) and a new cell cycle index $B(i, j/t)$. To account for a certain variance a prospective cell cycle time was selected at random within a certain range. Thus, stem cells can have a cycle time between 12 hr and 20 hr and transit cells between 10 hr and 14 hr.

(iv) Alternative calculations were performed with different cell phase durations.

### 3. Cell displacement

(i) There is a general vertical cell movement in the crypt (Leblond & Stevens, 1948; Quastler & Sherman, 1959; Cairnie *et al.*, 1965; Schmidt *et al.*, 1985; Wilson *et al.*, 1985). At the top of the crypt the cells move at about one position per hour (Cheng & Leblond, 1974; Al-Dewachi *et al.*, 1975; Potten & Hendry, 1983; Kaur & Potten, 1986a,b,c). The mechanisms generating this movement are not understood. Horizontal displacements have also been suggested to occur (Potten *et al.*, 1982), but could not be quantified. No information was available on whether or not this is a random or selected process.

(ii) In the model, cell displacement was assumed to be connected to mitotic activity. This was done without prejudicing particular mechanisms. We introduced a selection criterion for cell displacement based on local neighbourhoods

*Reference model (model E): local age-dependent displacement considering three neighbouring cells.* It was assumed that a newly formed daughter cell selects the oldest of the three immediate neighbour cells to the left, right or above and moves into that position shifting the rest of the selected column one cell position upwards (Fig. 1). 'Age' is used in the sense that a T3 cell is older than a T2, but also that a T3 cell in S phase is older than a T3 cell in $G_1$ phase; i.e. we measure the entire time a cell (line) has lived since its origin from a stem cell. If two equally old neighbours exist, one is selected at random. Lateral displacement was not allowed to displace a non-migratory P or A-cell.

(iii) The values of the matrices $A(i, j/t)$ and $B(i, j/t)$ were clearly changed when a new cell was placed at position $(i, j)$. $A(i, j/t)$ and $B(i, j/t)$ were defined by the generation and age index of the new cell and the cells above were then shifted one position upwards. The algorithm is straightforward.

(iv) In total, eight different displacement mechanisms were tested. They may be classified in order of increasing complexity. Mechanisms in which the dividing cell ignores local cellular neighbourhoods or environments (models A, B below) are the simplest cases. If the dividing cells are influenced by 'weak' local (C) or 'weak' global (D) criteria they must acquire some information about the status of other cells ('weak' here refers to non-immediate neighbour influences). If each dividing cell has to 'assess' the status of all its direct neighbours then complex mechanisms are evoked (E, F, G). Finally, we believe that the most rigorous assumption is an external trigger imposed on the system (a cut-off model) which assumes a more global knowledge by the cells of the whole crypt's status (H). The eight models considered are as follows. *Model A: Vertical displacement* only (i.e. no lateral movement): the column on top of a dividing cell is simply shifted upwards. Daughter cells are then always arranged vertically. *Model B: Random displacement:* one daughter cell is randomly shifted either left, right or upwards. The whole selected column is then shifted upwards. *Model C: Random displacement with a local mature cell dependent rearrangement at the transit/mature cell junction:* an extension of model B where the column movement is more complicated. Cells in a selected column are progressively shifted upwards unless the next neighbour to the left or right is an M-cell. In this case the cell is shifted below this M-cell and the rest of that column is then shifted upwards. *Model D: Long-range mature cell dependent displacement:* a new cell is placed into that column to the left, right, or above which has the most postmitotic M-cells. Processes as (C) and (D) shift M-cells from low positions to higher crypt regions. *Model E: Local age-dependent displacement with three neighbours:* See reference model (ii) above. *Model F Local age-dependent displacement with five neighbours:* a newly formed daughter cell selects the oldest neighbour to the left, top, right (as in model E) and also to the *top left and top right*. The rest of the selected column is then shifted upwards. *Model G: Successive local age-dependent displacements:* after a selection of displacement by the model E the evicted neighbour cell then undertakes a second age-dependent displacement according to model E etc. The local age-dependent displacement process was iterated five times. The final selected column of cells is then shifted upwards. *Model H: Random displacement with a cut-off point determining final maturation:* a random displacement was assumed as in model B. In addition an environmental influence was imposed determining the final differentiation of transit cells. Cells passing position 13 complete their present cell cycle after which they become postmitotic M-cells irrespective of their previous generation age. Consequently, not all differentiating cells undergo the same number of cell divisions.

Using the assumptions in (1)iii–(3)iii (above) the model crypt was operated for 500 hr before labelling was simulated. This eliminated any initial random effects. For each time-step the whole crypt was scanned for mitotic cells. The algorithm started at the top of the crypt and proceeded row by row. Once a mitotic cell was found the migration process was performed as described above. The scanning procedure then continued down to the bottom. Thereafter all cells aged by 1 hr and the whole process was repeated. For all subsequent evaluations at least 10 independent crypts were simulated and the model results were pooled, thereby corresponding to 160 experimental crypt sections.

In order to test whether the step size of 1 hr was too long, it was reduced by a factor of four in a series of simulations which did not produce different results. Therefore, the 1 hr step size was maintained which reduced the computer performance time to a practical level.

**4. LI labelling**

(i) A set of actual LI data was selected from current experiments which allowed the model to be tested. Tritiated thymidine was injected into mice at a dose of 25 $\mu$Ci per mouse at 09.00 hours. The percentage of labelled cells in the crypt (labelling index, LI) was measured in relation to cell

position. The LI was evaluated at 0·6, 3, 6, 9, 12, 24 and 48 hr after labelling (Fig. 3). The experimental data were obtained from 200 to 300 half crypt sections as described elsewhere (Potten *et al.*, 1982; Kaur & Potten, 1986a,b,c).

(ii) We assumed that all S phase cells could be equally labelled and that after division both daughters remain labelled. It was assumed that dilution of label was negligible. Paneth cells were assumed to remain unlabelled. M-cells could not initially be labelled, but labelled transit cells could become labelled M-cells in the course of time.

(iii) Whether a cell was labelled or not was described in a matrix $C(i, j/t)$. Daughter cells carried the same label as their mothers. At time $t = 0$ all cells in S phase were labelled by assigning their $C(i, j/t = 0)$ the value 1 (or 0). To identify cells in S phase, the matrices A and B were consulted. According to Fig. 1, the LI at position $j$ and time $t$ was defined as the row percentage of labelled cells

$$LI(j/t) = \underset{i=1,\ldots,16}{\text{Sum}} C(i, j/t)/16$$

Generally 10 model crypts (= 160 columns) were evaluated to determine the LI for each position at 0, 3, 6, 9, 12, 24, 48 hr after labelling.

**5. Runs**

(i) In a given longitudinal crypt section (column) one counts the number of labelled and unlabelled sequences (number of runs) from the bottom to the top (position 24) of the crypt (Fig. 1). This quantity, first introduced by Potten *et al.* (1982) is connected with the length of consecutive like-labelled cells; e.g. many single labelled cells lead to a large number of runs while long sequences of labelled or unlabelled cells lead to a small number of runs. The initial number of runs depends on the length of the S phase and the degree of synchrony between daughter cells. Changes in the number of runs with time gives information about the lateral displacement of labelled and unlabelled cells, since this would break up long sequences.

(ii) In the model the number of runs was evaluated in each column and their relative frequency was determined. As the top and bottom of a column consists of unlabelled M- and P-cells respectively, the number of runs in the model is always odd. In order to compare the number of runs with the data, the frequency of consecutive odd and even number of runs was always pooled (RUN(0) + RUN(1), RUN(2) + RUN(3) etc.). Furthermore, numbers of runs were only evaluated between position 1 and 24; i.e. only within the crypt.

(iii) The number of runs in column $i$ is calculated from

$$RUN(i/t) = 1 + \underset{j=1,\ldots,24}{\text{SUM}} \{ABS[C(i, j+1/t) - C(i, j/t)]\}; \quad \text{where } C(i, j \geqslant 25/t) = 0$$

**6. Frequency of lateral cell displacements**

(i) The frequency of lateral cell displacements is not known.

(ii) In the model the frequency of lateral displacement can easily be calculated. For each cell division it can be recorded whether the cell displacement was vertical or lateral.

(iii) Alternative displacement mechanisms can be compared with one another if all other parameters are kept the same (Table 3 below).

## MODEL RESULTS

In order to quantitatively test the validity of several biological assumptions on the crypt proliferative system, we performed model calculations which can be compared to actual data from the ileum. We present results of different scenarios. The simulations in paragraph I (below)

**Table 3.** Alternative cell displacement processes

| Displacement process | Model agreement with data | |
|---|---|---|
| | LI | RUN |
| Acceptable models | | |
| E Local age-dependent displacement with three neighbours (reference model) (Figs 3, 4 full lines) | +++ | + (42%)* |
| F Local age-dependent displacement with five neighbours (Figs 3, 4 dashed lines) | + | +++ (80%)* |
| H Random displacement with cut-off at position 13 | ++ | ++ (63%)† |
| Rejectable models | | |
| A Vertical displacement (Fig. 5a) | ++ | − (0%)* |
| G Successive local age-dependent displacement | + | − (19%)* |
| C Random displacement with local M/T rearrangement | − | ++ (64%)* |
| B Random displacement (Fig. 5b) | − | ++ (65%)* |
| D Long-range mature cell dependent displacement | − | +++ (80%)* |

* In brackets: % of newly produced cells that are shifted into lateral columns. On average 420 cell divisions take place per day in the model crypt.

† On average about 390 cells divide per day per model crypt.

are based on the reference model (E) and a particular set of reference parameters (see below). Subsequently (II) we present model simulations where either different displacement models (using the same set of reference parameters), or modified sets of parameters (within the reference displacement model) were chosen.

**I. Reference model (E) and reference parameters**

The seven fundamental model parameters for the reference model (E) were as follows (see Tables 1 and 2): (a) Paneth cells are distributed between crypt position 1 and 6, hence stem cells are distributed between positions 2 and 7; (b) each crypt has sixteen stem cells (one per column) ($N_A = 16$); (c) the stem cell average $T_C$ is 16 hr (range: 12–20 hr); ($T_{CA} = 16$ hr); (d) the stem cell $T_S$ is 9 hr; ($T_{SA} = 9$ hr); (e) four proliferating transit generations exist ($L = 4$); (f) the transit cell average $T_C$ is 11 or 12 hr (11 hr for the last two divisions, 12 hr for the first two) ($T_{CT} = 12, 11$ hr); (g) the transit cell $T_S$ is 8 hr ($T_{ST} = 8$ hr). $T_M$ is arbitrarily fixed at 1 hr for all cells.

*I.1 Crypt matrix*

Figure 1 shows an example of the crypt matrix directly after labelling.

*I.2 Family tree*

From the model it is possible to investigate to what extent the members of a particular family tree (i.e. all cells produced from one stem cell) move in relation to each other and the crypt as a whole, and to what extent lateral movement of the stem cell-derived families takes place. This cannot at present be investigated experimentally. The predicted pattern of lateral spreading in the reference model is shown in Fig. 2. The dots represent six stem cells at position 5. The full lines encircle the areas within which 90% of a particular generation of descendand transit cells can be found (full lines for model E, dashed lines for model F). Thus, for example, T2 cells are found in the three cell positions above the stem cell while T4 cells spread between cell position 8 and 19 and five adjacent columns. Mature progeny of one stem cell spread out over 5 to 7

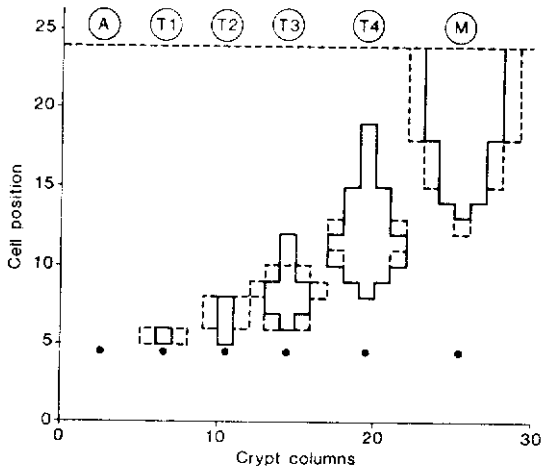


**Fig. 2.** The distribution of the offspring from individual stem cells (●). Within the areas indicated by the lines 90% of the cells of a particular transit or mature cell generation would be found. For simplicity, different generations have been separated from each other. Therefore, six stem cells are indicated on the bottom. The mature descendents of a stem cell can be found above position 13 spreading over 5 to 7 columns (right case). T4-cells in contrast spread over 5 columns between position 8 and 19, etc. Note that the different areas show overlaps indicating that mixtures of different generations can be found at most positions. The full lines show the transit cell family for the reference model (E). Somewhat broader families are obtained for model F (---), and model H is similar to model F.

columns while moving to the top of the crypt. One should note the overlap between the different generations. At each cell position a mixture of cells with different maturity can be expected.

*I.3 LI distribution and its movement up the crypt*

Figure 3a–g shows the measured position-dependent LI distributions at 0–48 hr after labelling (triangles). With time, labelled cells appear at higher crypt positions. The full lines represent the reference model predictions. All main characteristics of the data are reproduced, e.g. the shape of the curve, the height and position of the maximum and the displacement of the leading edge with time. Only some of the fine structure is not reproduced precisely. The excellent fit of model E to the LI data was the main reason for selecting it.

Figure 3h shows how the leading LI edge in Fig. 3a–g moves with time. The results were evaluated from the cell position at which the LI was 30% (about half the peak height position). There is good agreement between the data and the model. Both indicate a vertical velocity of about 1 cell position/hour ((position 38–position 16)/24 hr = 0·91 hr).

*I.4 The number of runs of labelled and unlabelled cells and their relevance for the quantification of lateral movement*

Figure 4a–g show the data obtained for the distributions of the number of runs between crypt position 1 and 24 over the period 0–48 hr after labelling. It is important to note that at least for 24 hr the position and shape of the measured distributions hardly change (triangles). The maximum remained stable at 8–10 runs. The subsequent analysis using the model reveals that this experimental finding has major implications for the type and quantity of lateral cell

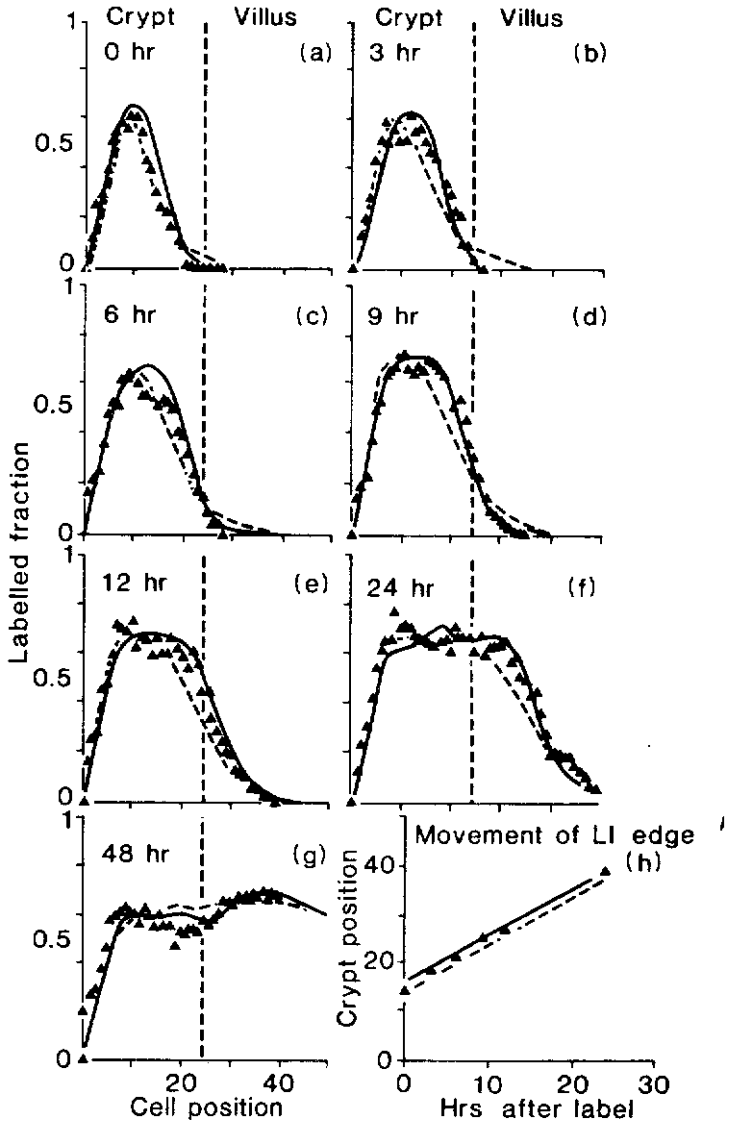


**Fig. 3.** LI-distributions. (a)–(g) Experimental data (▲) for the LI are shown for various times (0, 3, 6, 9, 12, 24, 48 hr) after [$^3$H]TdR administration (25 $\mu$Ci given at 09.00 hours). Model curves generated by the two local age-dependent displacements processes are shown for comparison (——: reference model E, 3 neighbours; – – –: model F, 5 neighbours). The reference model E shows a better fit, especially of the shape of the leading LI edge. The cut off model H would generate curves intermediate to models E and F, provided all other parameters remain the same. The LI curves show a movement of the leading edge. The position of the 30% LI value can be related to the time after labelling (Fig. 3h). Data (▲) and model curves (——: model E, – – –: model F) show good agreement indicating a movement of 1 cell position per hour.

displacements. The full lines in Fig. 4a–g again show the curves generated by the reference model. They reproduce the shape of the distributions and remain at a constant position for 24 hr, but the model consistently generates too few runs (the maximum is 6). However, we consider the fit to be reasonable (see also below).

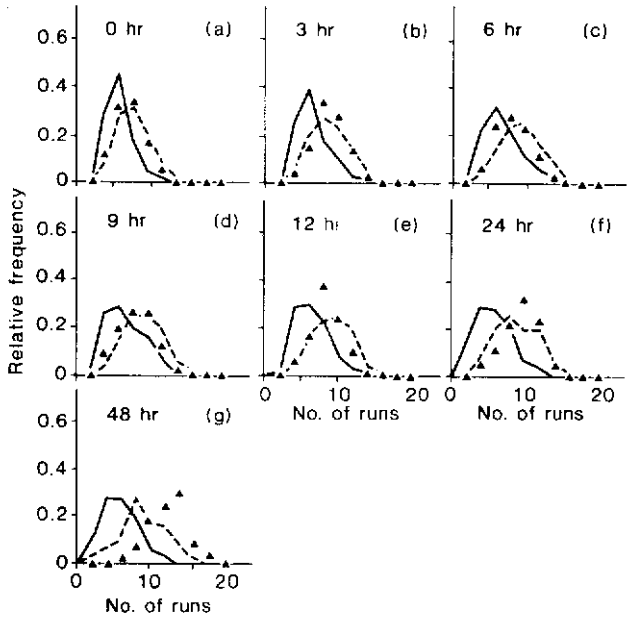


**Fig. 4.** RUN-distributions. In crypt sections (i.e. a column in the model; see Fig. 1) one can evaluate how often the series of similarly labelled cells change. As this is done for many sections (columns), a frequency distribution of the percentage of all runs of a particular value (e.g. 0·33 of all crypt columns had 7 runs) is obtained. Experimental data (▲) and model curves are shown for various times (0.6, 3, 6, 9, 12, 24, 48 hr) after labelling. The reference model curves (model E), (——) have the same shape as the data but differ in the average values. Curves generated by model F fit the data very well (– – –). The cut off model H produces curves similar to model F but positioned slightly to the left.

## II. Alternative assumptions

### *II.1 Alternative displacement mechanisms*

Any newborn cell must be positioned adjacent to its mother cell but several alternative possibilities can be envisaged. We tested eight different displacement processes. They influence LI and run distributions to different degrees. Table 3 summarizes the findings. The models are discussed in a sequence according to increasing complexity.

(1) In the first two models environment or neighbourhood conditions are neglected. *Model A: Only vertical displacement*: the model produces good fits to the LI data, but it can be rejected because it leads to a progressive fall in the number of runs with time. This can be understood as all new daughter cells would always be placed on top of each other. Thus, for example, after two divisions an originally labelled mother cell gives rise to a quadruplet of equally labelled cells. Consequently long sequences of equally labelled cells result and the run distribution would shift to the left and this is inconsistent with data (see Fig. 5a). *Model B: Random displacements*: although this model produces good fits to the run data, it must be rejected because it generates long tails in the LI distributions with a flat slope to the leading LI edge (Fig. 5b). A random displacement would sometimes place young transit cells below other young cells resulting in a large amplifying potential in that column (i.e. M-cells will occur only at very high positions). Conversely, the original column having lost a young cell would produce postmitotic cells too early (i.e. M-cells at low positions). Figure 6 shows that transit cells may be found anywhere between position 13 and 40, i.e. there is no well-defined boundary between transit and mature

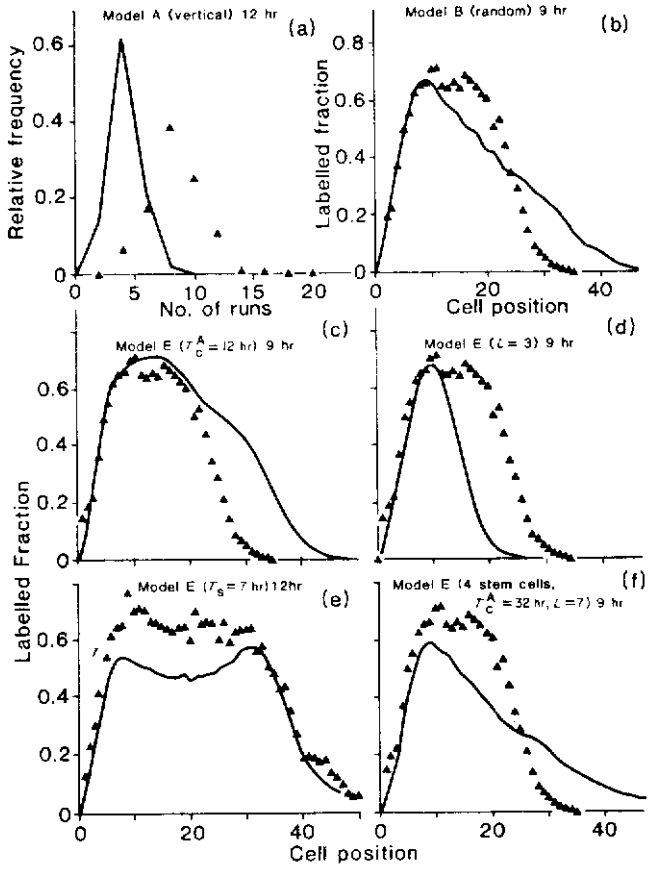


**Fig. 5.** Examples of alternative assumptions (— = model predictions; ▲ = actual data). (a) Run distribution for the vertical displacement mechanism (A) (9 hr after labelling). As cells remain vertically adjacent after division the process tends to generate long runs of equally labelled cells. The theoretical run distribution therefore favours small numbers of runs quite unlike the real situation. (b) LI distribution for the random displacement mechanism (B). The flat leading edge (long tail) does not fit the data (9 hr after labelling). (c) LI distribution for the age-dependent displacement (E) with a reduction in the stem cell cycle time to 12 hr. The velocity of the leading edge of the LI distribution is much faster than that in the data (9 hr after labelling). (d) LI distribution for the age-dependent displacement (E) with three transit populations. The velocity of the leading edge of the LI distribution is now too slow compared with the data (9 hr after labelling). (e) LI distribution for the age-dependent displacement (E) with a reduction in $T_S$ of transit cells to 7 hr. The plateau value of the LI is now too small (24 hr after labelling). (f) LI distribution for the age-dependent displacement (E) with four stem cells per crypt, seven transit populations and a stem cell cycle time of 32 hr. The flat leading edge (long tail) does not fit the data (9 hr after labelling).

cells. Apparently this model does not produce a good position-related age ordering in the crypt. An ideal age ordering would be the case if at a particular crypt position only identical transit cells were present with increasing maturity at higher positions. However, in this model all types of T-cells can be found at any position.

(2) Next, there are those processes that involve weak local or global selection criteria. *Model C: Random displacement with local T/M rearrangement*: this is basically a random process with additional conditions which should tend to stabilize the boundary between transit and mature

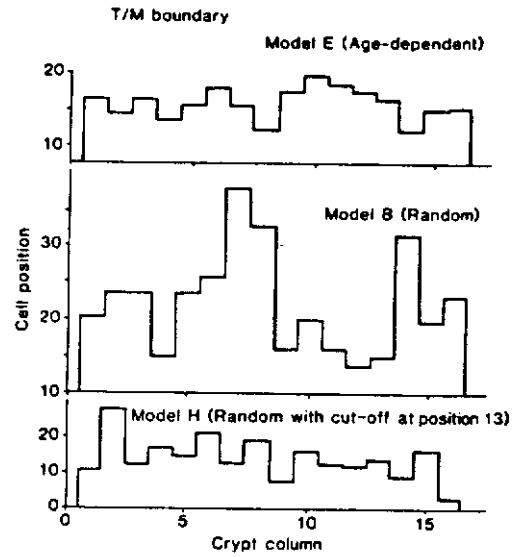


**Fig. 6.** The positions of the highest transit cells (the T/M boundary) in model crypts are shown for model E (top), model B (middle), model H (bottom).

cells. *Model D: Long range M-cell dependent displacement*: this is a sort of long range feedback leading to a supply of cells to those columns which have many M-cells. It was our initial speculation that both mechanisms might introduce some position-related age ordering within the disorganized crypt expected on the basis of initial random displacement. The simulations, however, reveal that this is not the case. The LI distributions never fit the data particularly well, although there is a better fit to the run data. Both models generate curves very similar to model B.

(3) Then, there are those processes that involve strong local neighbourhood selection criteria. The local age-dependent selection processes (models E, F, G) are mechanisms which effectively produce a situation where older cells tend to sit on top of younger cells, thus providing rather strict position-related age ordering. Consequently the boundary between transit and mature cells is relatively sharp, i.e. the leading LI edge is rather steep. As already shown in Fig. 3a–g the fit of model E to LI data is excellent. Model F generates curves, also displayed in Fig. 3 (dashed lines) which are good fits also, but not quite as good as for model E; e.g. the leading LI edge is less steep for model F. In contrast, model G with its iterated age criterion generates curves with LI edges which are too steep.

The differences between models E, F and G are more pronounced with respect to the run distributions. Figure 4 has already presented the unsatisfactory aspects of model E. Model F generates an excellent fit to run data. In contrast, model G produces run curves comparable to model A (similar to Fig. 5a) and therefore must be rejected.

The mechanisms involved in model G result in a very strict position-related age ordering in the crypt such that older cells in a neighbourhood are generally found on top of dividing cells. The age-dependent displacement therefore is primarily vertical. Table 3 shows that only 19% of all new-born cells are shifted into lateral columns, while 42% do so in model E and 80% in model F where the probability of lateral displacements is higher. This clearly shows that the amount of lateral displacement is related to the positioning of the run distribution.

(4) Finally, there is a fourth category where a maturation determination (a cut-off process) may be superimposed on any of the above displacement mechanisms. Model H is a combination

of the random process B with a 'cut-off' mechanisms. Such a model assumes an environmental factor which 'repairs the chaos' produced by the random mechanism lower down the crypt. The model by definition does not allow for transit cells at high positions (see Fig. 6). It generates good overall fits to both the LI data and run distributions (see Table 3). The LI curves would lie between those for models E and F (see Fig. 3). Typical run-distributions would be similar to those for model F but are still slightly to the left of the actual data.

*II.2 Alternative parameters*

In order to test how changes in the basic cell kinetic parameters effect the model, we have used our reference model E and varied several of the parameters. The influence of such changes are similar whichever of the migration models are selected.

One of the major conclusions from this analysis is that the run distributions are rather insensitive to parameter changes while the shape of LI curves can be easily affected. The run distributions generally only start to change after the LI curves show drastic alterations. We therefore restrict the subsequent discussion to the LI curves.

(1) *Change in only one parameter (see I).* Acceptable LI curves are generated under the following conditions: (a) any Paneth cell distribution where the P cells lie between crypt position 1 and 7, so that the stem cells are spread over at least three positions (e.g. 3–5, 1–5, 3–7); (b) 14–16 stem cells per crypt. More than sixteen stem cells cannot be simulated in the model; fewer reduce the velocity of the LI edge; (c) 14–18 hr for the average $T_C$ of stem cells. A reduction (e.g. to 12 hr) increases the velocity of the leading LI edge (see Fig. 5c); (d) 8–10 hr for the $T_S$ of stem cells. Alternative times will change the LI curves particularly at low crypt positions eventually resulting in unacceptable peaks or troughs; (e) no integer change up or down in the number of transit generations (L) is acceptable. Figure 5d shows that three transit generations result in curves that do not fit the LI data. If fractional average numbers of generations are considered then the average number of transit mitoses must be between 3·8 and 4·2; (f) 10–13 hr for the average $T_C$ of transit cells. The use of two $T_C$ subsets for the T-cells is somewhat secondary. It was introduced to improve the fit to the 24 and 48 hr LI data; (g) 8–9 hr for the $T_S$ of transit cells. Figure 5e shows that reducing this $T_S$ to 7 hr reduces the plateau of the LI curve in an unacceptable fashion.

(2) *Changes in several parameters.* In order to obtain a good fit to the LI data, it is a necessary condition that the velocity of the leading LI edge is reproduced. According to the appendix (eqn 4), any combinations of stem cell numbers per column ($N_A$), their cycle time ($T_{CA}$) and the number of transit generations ($L$) fulfilling the equation 1 cell position/hr $= 2^L * N_A/T_{CA}$ may be suitable. For integer values of $L$ the thick lines in Fig. 7 indicate the possible choices. However, not all combinations are acceptable for the following reasons: (a) due to the architecture of the crypt, it is unlikely that more than sixteen active stem cells can be stably arranged in a sixteen-column circumference; (b) from general eukaryotic cell kinetic considerations, it is unlikely that the stem cells have a cell cycle shorter than 8 hr. Thus, the dark shaded regions in Fig. 7 *a priori* can be excluded as possible stem cell parameters. The following restrictions are based on model analyses where $L$, $N_A$, $T_{CA}$ were systematically changed. If these changes resulted in unacceptable LI distributions, the parameters could again be rejected; (c) stem cell cycle times ($T_{CA}$) under 12 hr; (d) a prolongation of $T_{CA}$ beyond 32 hr generally produced flat LI curves with long tails (similar to Fig. 5b); (e) a reduction of the stem cell number so that more than six transit divisions are necessary to maintain the crypt output also led to inadequate LI curves. Figure 5f shows such an example (four stem cells ($N_A = 0{\cdot}25$), $T_{CA} = 32$ hr and $L = 7$).

The range (areas) of parameters excluded by our model analyses are indicated in Fig. 7 by the light shading. The remaining 'window' (unshaded box) shows the currently acceptable

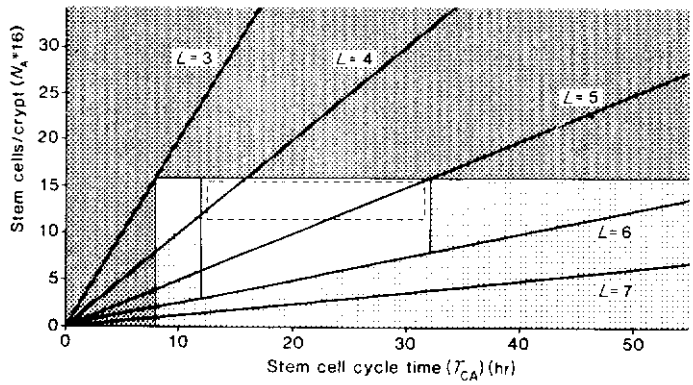


**Fig. 7.** In this diagram the number of stem cells per crypt ($N_A$) and their cycle time ($T_{CA}$) represent the $y$ and $x$ axis. In order to produce 1 cell per hour at the top of the crypt, the number of transit generations ($L$), $N_A$, $T_{CA}$ have to fulfill the condition 1 cell position/hr = $2^L \cdot N_A/T_{CA}$. In the reference model this is satisfied when $L = 4$, $N_A = 1$ (= 1 stem cell per column) and $T_{CA} = 16$ hr. Other acceptable combinations for $L = 4$ are located on the corresponding thick curves. For more transit populations (e.g. $L = 5, 6$) the relations are also indicated. However, not all combinations are acceptable. More than sixteen stem cells per crypt cannot stably be situated at the crypt circumference. Eukaryotic cycle times shorter than 8 hr can also be excluded (■). Based on simulations using the reference model a stem cell with $T_{CA}$ shorter than 12 hr or larger than 32 hr can be excluded. Fewer than four stem cells or other conditions that would demand more than six transit divisions are also unlikely (⊡). The remaining window (□) includes the range of acceptable parameter combinations. The window is smaller for model F (---) and larger for model H (up to $T_C = 48$ hr and $L = 7$ but not below four stem cells per crypt).

parameters using model E. If fractional average numbers of transit divisions are accepted then all the range of parameters within this window is acceptable. Similar windows can also be obtained for other models. Model F would have a much smaller window (dashed lines in Fig. 7) while model H could allow a larger spectrum of parameters than model E (up to $L = 7$ and $T_{CA} = 48$ hr). One should finally note that none of the models examined works if less than four stem cells per crypt are assumed.

## DISCUSSION

It was the purpose of this work to bring our knowledge on steady-state crypt proliferation within a quantitative framework. This would allow a rigorous testing of biological concepts and should provide new interpretations of available data as well as predictions for future experiments. At the start of this investigation precise values on ileal crypts were available for only a few parameters: (1) the vertical migration velocity at the top of the crypt (1 position/hr); (2) the cell cycle times of the transit cells (from PLM: $T_C = 12$ hr, $T_S = 7$–9 hr, and $T_{G_2+M} = 2$–3 hr); (3) the number of proliferating and mature cells per crypt; (4) the number and distribution of Paneth cells. However, the number of stem cells, the cell cycle times of the stem cells, and the number of mitoses in the transit cell population were uncertain. In addition there was little information available about the mechanisms involved in the migration process, for example about the amount of lateral cell displacement.

In an attempt to clarify some of these points we made use of Monte Carlo simulations with models of the individual cell distributions in the intestinal crypt. By testing a variety of models we have shown that strictly local age-dependent displacements of newborn cells (models E, F) can explain both the LI and run data in murine crypts; i.e. the intestinal crypt cells apparently

behave in a way suggesting that they sense the maturity or age of local surrounding cells. It appears that each cell would only need a knowledge of the age status of its immediate neighbours and that other environmental controls are not necessary. However, the number of divisions differentiating transit cells undergo must then be predetermined (e.g. four).

These local age assessments would produce a certain position-related age ordering in the crypt such that older (more differentiated) cells are usually found above younger cells. We showed that the steepness of the upper edge of the LI distributions suggests a fairly strict position-related age ordering in the crypt. However, the order would be perturbed by any lateral shifting of cells. We estimate from the run data that lateral cell displacements occur about 250 to 350 times per day, i.e. after 60 to 80% of the 420 daily mitoses in the model crypt. However, the ordering force (of the local age-dependent displacement) compensates for this 'mixing' process.

The number of mitoses per day and indeed the number of cells in the model crypt matrix (Fig. 1) are both somewhat greater than is believed to be the actual situation (see Potten & Hendry, 1983; Potten *et al.*, 1983; Wright & Alison, 1984). This is partly because we have not considered goblet cell differentiation which probably prematurely extinguishes branches of the cell lineage. It is also partly due to the fixed position assumed for the crypt–villus junction in the case of the matrix, and finally may be due to the fact that crypts may have a circumference of less than sixteen cells in mid-crypt positions.

The best fits to the data considering all three acceptable models (E, F and H) were obtained with sixteen stem cells ($T_{CA} = 16$ hr, $T_{SA} = 9$ hr and four transit generations ($T_{CT} = 11$–$12$ hr, $T_{ST} = 8$ hr) (i.e. the reference model parameters). Reasonable fits were also obtained for some different combinations of parameters (see windows in Fig. 7). It seems likely that local displacement criteria for cell migration only work if more than four stem cells with a $T_{CA}$ between 12 and 32 hr are present in a crypt.

The cut-off model (H) is a good alternative to the local age-dependent mechanisms (E, F). The main difference is that in the cut-off model the number of transit generations is not predetermined but is determined by extracellular factors. A decision between the local and the cut-off models is not possible on the basis of steady-state studies of LI and runs. It is, however, likely that data from perturbed situations (e.g. after irradiation) may clarify the question. Conceptually we prefer the local model because the mechanisms seem biologically simpler. Each cell would only need knowledge about its immediate neighbours while the cut-off model requires an integrated knowledge of the total crypt (e.g. number of transit cells).

The two types of model explain virtually all the cell kinetic data for the crypt after labelling with 25 $\mu$Ci [$^3$H]TdR at 09.00 hours. This holds true even though some assumptions may be severe oversimplifications of the real situation. Firstly, the shape of a crypt may not be cylindrical, not all crypts may have exactly the same length and circumference, and many experimental sections may not be parallel to the axis of the crypt, nor will the cells all have the same size. Different crypt shapes or other lattices (e.g. hexagonal) could be used but are not suspected to produce basically different results. Secondly, we considered only three different cell cycle times within the proliferative compartment. There may be a greater heterogeneity related to the cell position. Thirdly, we neglected cell death and the differentiation of goblet cells. Fourthly, we neglected any perturbations that might be induced by tritiated thymidine. Fifthly, circadian rhythms were neglected. LI data after labelling at other times of the day indicate a small circadian rhythm. Modelling to include these phenomena is currently in progress.

An implication of eqn 4 in the appendix is that if independent information about the number of transit generations was available, the number and cycle time of stem cells could be more accurately defined.

There is a stochastic element in the models. The curves predicted by the model suffer from

'sampling errors' similar to those in actual experiments. Minor discrepancies between the model curves and the data may well be attributed to this effect. The 48 hr LI data (Fig. 3g) exhibits a trough at about the 20th cell position which might be attributed to heterogeneity in cycle times of transit cells (shorter $T_C$ for more mature transit cells). It must, however, be noted that the geometry of the villus is not properly taken into account in this model and that all fits in this region may be completely fortuitous. The 48 hr RUN data distribution is shifted to the right (Fig. 4) and none of our simulations fitted these data well. Other considerations may need to be taken into account here (e.g. circadian rhythm, thymidine effects). Some experimental sections may cut two or three crypt columns. This would induce a slight overestimation of the actual number of experimental runs by 1 or 2 which does not change the above conclusions. It should be noted that the duration of the mitotic phase (1 hr) will be examined more accurately in conjunction with a forthcoming analysis of mitotic index data.

To our knowledge this analysis presents the first comprehensive model description of the two-dimensional cell layer in crypts. A conceptually similar one-dimensional model was recently published to fit LI data (Meinzer & Sandblad, 1985a,b). It describes only one crypt column without lateral cell exchange and therefore is equivalent to a pure vertical displacement (model A) which fits LI but fails to fit the run-data (see Fig. 5a).

In summary, we present a comprehensive model for the crypt which permits a consolidation of information on the number of stem cells, transit cells, cycle times and the kinetic and migratory properties of the daughters of stem cells. In particular the modelling has permitted a new understanding of the probable processes involved in the migration of cells in the epithelium. Furthermore, a new interpretation of LI and run data (in a moving cell layer) was achieved which demonstrated that the LI carries information on the position-related age ordering of transit cells and the run distributions on the frequency of lateral cell displacements. Such information could only be obtained by the model approaches adopted here. Further papers in preparation will demonstrate that a wide range of experimental data (PLM, mitotic indices, continuous labelling experiments) can also be analysed and that minor or major perturbations (e.g. circadian rhythms and cytotoxic insults) can subsequently be considered.

## ACKNOWLEDGMENTS

We thank Juergen Glatzer for performing the final computer calculations and graphics and providing stimulating discussions. We are grateful to Stephan Gontard for typing the manuscript, to Ursula Paulus for reading the manuscript and to Caroline Chadwick for her help with some of the experiments. Our work is supported by the Volkswagenstiftung (FRG) and the Cancer Research Campaign (U.K.).

## REFERENCES

AL-DEWACHI, H.S., APPLETON, D.R., WATSON, A.J. & WRIGHT, N.A. (1979) Variation in the cell cycle time in the crypts of Lieberkuehn of the mouse. *Virchows Arch Cell Path.* **31**, 37.

AL-DEWACHI, H.S., WRIGHT, N.A., APPLETON, D.R. & WATSON, A.J. (1975) Cell population kinetics in the mouse jejunal crypt. *Virchows Arch Cell Path.* **18**, 225.

CAIRNIE, A.B., LAMERTON, L.F. & STEEL, G.G. (1965) Cell proliferation studies in the intestinal epithelium of the rat. I. Determination of the kinetic parameters. *Exp. Cell Res.* **39**, 528.

CHENG, H. & LEBLOND, C.P. (1974) Origin, differentiation and renewal of the four main epithelial cell types in the mouse small intestine. *Am. J. Anat.* **141**, 461.

DEVIK, F. & HAGEN, S. (1973) Effects of X-rays and cytotoxic agents on the cell population of the crypts of the small intestine in mice. *Virchows Arch. Abt. Cell Path.* **12**, 223.

DEVIK, F. & IVERSEN, O.H. (1970) Observations on the generation time of Paneth cells in mice. *Virchows Arch.* **4**, 191.

KAUR, P. & POTTEN, C.S. (1986a) Circadian variation in migration velocity in small intestinal epithelium. *Cell Tissue Kinet.* **19**, 591.

KAUR, P. & POTTEN, C.S. (1986b) Cell migration velocities in the crypts of the small intestine after cytotoxic insult are not dependent on mitotic activity. *Cell Tissue Kinet.* **19**, 601.

KAUR, P. & POTTEN, C.S. (1986c) Effects of puromycin, cycloheximide and noradrenaline on cell migration within the crypts and on the villi of the small intestine: a model to explain cell movement in both regions. *Cell Tissue Kinet.* **19**, 611.

KOVACS, L. & POTTEN, C.S. (1973) An estimation of proliferative population size in stomach jejunum and colon of DBA-2 mice. *Cell Tissue Kinet.* **6**, 125.

LEBLOND, C.P. & STEVENS, C.E. (1948) The constant renewal of the intestinal epithelium in the albino rat. *Anat. Rec.* **100**, 357.

MEINZER, H.P. & SANDBLAD, B. (1985a) A simulation model for studies of intestine cell dynamics. *Comp. Prog. Biomed.* **21**, 85.

MEINZER, H.P. & SANDBLAD, B. (1985b) Simulation of cell kinetics in the intestinal tract. In: *Med. Informatics Europe 85* (Eds F. H. Roger *et al.*), pp. 479–483. Helsinki, Springer, Berlin.

POTTEN, C.S., KOVACS, L. & HAMILTON, E. (1974) Continuous labelling studies on mouse skin and intestine. *Cell Tissue Kinet.* **7**, 271.

POTTEN, C.S. & HENDRY, J.H. (1983) Stem cells in murine small intestine. In: *Stem Cells: Their Identification and Characterisation* (Ed. C. S. Potten), pp. 155–199. Churchill-Livingstone, Edinburgh.

POTTEN, C.S., HENDRY, J.H., MOORE, J.V. & CHWALINSKI, S. (1983) Cytotoxic effects in gastro-intestinal epithelium (as exemplified by small intestine). In: *Cytotoxic Insult To Tissue* (Eds C. S. Potten & J. H. Hendry), pp. 105–152. Churchill-Livingstone, Edinburgh.

POTTEN, C.S., CHWALINSKI, S., SWINDELL, R. & PALMER, M. (1982) The spatial organization of the hierarchical proliferative cells of the crypts of the small intestine into clusters of 'synchronized' cells. *Cell Tissue Kinet.* **15**, 351.

QUASTLER, H. & SHERMAN, F.G. (1959) Cell population kinetics in the intestinal epithelium of the mouse. *Exp. Cell Res.* **17**, 420.

SCHMIDT, G.H., WILKINSON, M.M. & PONDER, B.A.J. (1985) Cell migration pathway in the intestinal epithelium: an *in situ* marker system using mouse aggregation chimaeras. *Cell*, **40**, 425.

TSUBOUCHI, S. & POTTEN, C.S. (1985) Recruitment of cells in the small intestine into rapid cell cycle by small doses of external alpha or internal beta radiation. *Int. J. Radiat. Biol.* (in press).

WILSON, T.J., PONDER, B.A.J. & WRIGHT, N.A. (1985) The use of a chimaeric model to study cell migration patterns in the small intestinal epithelium. *Cell Tissue Kinet.* **18**, 333.

WRIGHT, N.A. & ALISON, M. (1984) *The Biology of Epithelial Cell Populations*, Vol. 2. Clarendon Press, Oxford.

## APPENDIX

It is helpful to consider an extremely simplified model which neglects lateral displacements. For such a one-dimensional model, restricted to one column, one can introduce further simplifying assumptions to obtain precise formulae relating the number of transit divisions ($L$), the number of stem cells per column ($N_A$) and their cycle time ($T_{CA}$) to the velocity and position of the leading LI edge. In steady state the influx to generation compartment $i+1$ equals twice the influx to generation compartment $i$ per time interval. For $i = A$ (i.e. for stem cells) the efflux is split into two parts: one enters generaton 1 (i.e. T1) and one remains in the stem cell compartment. Thus, the stem cell compartment retains its size. Equation (1) describes the steady-state production rates:

$$\frac{N_1}{T_{C1}} = \frac{N_A}{T_{CA}} \qquad (1)$$

$$\frac{N_{i+1}}{T_{Ci+1}} = 2 \cdot \frac{N_i}{T_{Ci}}$$

$i = 1, \ldots, L$; $L+1$ represents the M-cells, $N_i$ is the number of transit cells of generation $i$ per column and $T_{Ci}$ are the corresponding cell cycle times. By induction one gets the general equation

$$N_i = 2^{i-1} \cdot T_{C_i} \cdot \frac{N_A}{T_{CA}} \tag{2}$$

The velocity of a cell at the boundary between T and M-cells is determined by the number of cells being produced by cells at lower positions. Consequently one obtains

$$V(L, L+1) = \frac{N_A}{T_{CA}} + \frac{N_1}{T_{C1}} + \cdots + \frac{N_L}{T_{CL}} \tag{3}$$

By virtue of eqns (1) and (2) it follows that

$$V(L, L+1) = (1 + 1 + 2 + \cdots + 2^{L-1}) \cdot N_A / T_{CA}$$

which can be summed up to

$$V(L, L+1) = 2^L \cdot N_A / T_{CA} \tag{4}$$

This formula is important because it explains that the velocity of the leading LI edge is determined by the stem cell efflux and the number of transit divisions alone. In the steady state the cell cycle time of transit cells does not play a role. Therefore the migration velocity of the leading LI edge is directly related to the combination of stem cell number, cycle time and number of transit generations (see Fig. 6).